materials

MDPI

Article

Effect of Ultraviolet–Ozone Treatment on the Properties and Antibacterial Activity of Zinc Oxide Sol-Gel Film

Ji-Hyeon Kim [1], Junfei Ma [1,2], Seunghun Lee [1], Sungjin Jo [2] and Chang Su Kim [1,*]

[1] Advanced Nano-Surface Department, Korea Institute of Materials Science, 797, Changwon-daero, Sungsan-gu, Changwon 51508, Korea

[2] School of Architectural, Civil, Environmental, and Energy Engineering, Kyungpook National University, Daegu 41566, Korea

* Correspondence: cskim1025@kims.re.kr; Tel.: +82-55-280-3696

Received: 2 July 2019; Accepted: 24 July 2019; Published: 29 July 2019

Abstract: To combat infectious diseases, zinc oxide (ZnO) has been identified as an effective antibacterial agent; however, its performance can be adversely affected by harsh application environments. The ozone impact on ZnO antibacterial film needs to be evaluated prior to its application in an ozone disinfection system. In this study, ZnO films synthesized via sol-gel/spin-coating were subjected to ultraviolet–ozone (UVO) treatment for different periods. Surface investigations using scanning electron microscopy, ultraviolet–visible spectroscopy, and X-ray photoelectron spectroscopy revealed that the treatment-induced film changes. With longer UVO treatment, the surface porosity of the film gradually increased from 5% to 30%, causing the transmittance reduction and absorbance increase in visible-light range. Phase transformation of $Zn(OH)_2$ to ZnO occurred during the first 10 min of UVO treatment, followed by oxygen uptake as a consequence of the reaction with reactive oxygen species generated during UVO treatment. However, despite these surface changes, the satisfactory antibacterial activity of the synthesized ZnO film against *Staphylococcus aureus* and *Escherichia coli* was sustained even after 120 min of UVO treatment. This indicates that the UVO-induced surface changes do not have a significant effect on the antibacterial performance and that the ZnO sol-gel film possesses good functional durability in ozone environments.

Keywords: zinc oxide; antibacterial film; sol-gel film; UV–ozone effect; film surface investigation

1. Introduction

Today, infectious diseases as well as environmental pollution have drawn attention worldwide. Particularly, hospital-acquired infections (called nosocomial infections) that occur in the hospital or other healthcare locations are considered an inevitable challenge for public health [1–7]. Nosocomial infections are estimated to annually result in at least 138,000 deaths worldwide, according to a report by the World Health Organization [8]. Accordingly, for the last two decades, antibacterial coatings along with antibiotics have been developed to prevent nosocomial infections and subsequent mortality. As major antibacterial agents depress the proliferation, spread, and infection of diverse strains, metal oxides such as ZnO [9–17], CuO [13,16,18], TiO_2 [19], Fe_2O_3 [13], Ag_2O [20], CaO [11], and MgO [11,21,22] have been extensively researched.

Among the metal-oxide agents, zinc oxide (ZnO) has been recognized as one of the promising antibacterial agents thanks to its inherent characteristics, such as good biocompatibility with humans (non-toxicity), biological effectiveness for bacteria-cell killing, low cost, and excellent physicochemical and thermal resistance—enabling its longer lifetime and higher cost-effectiveness than other organic and inorganic materials [12,23–30]. It has been proposed that the antibacterial effect of ZnO is attributed

to its three major antibacterial mechanisms: (1) formation of reactive oxygen species (ROS) [9,11,25]; (2) liberation of antibacterial ions—mainly Zn^{2+} ions [30–32]; and (3) internalization into the cell wall of strains, destroying the structural and functional integrity of the cell [23,33,34].

It has been experimentally verified that the performance of the ZnO antibacterial material is considerably affected by a variety of parameters, for example, its composition and structural properties (thickness for film structure, mechanical size for particle form, morphology, porosity, surface defects, and impurities) associated with the specific surface area [9,10,12,16,24,25,28,29,35–37]. These parameters can be influenced by the coating method. To synthesize high-quality ZnO films, many fabrication methods such as sol–gel [38–41], atomic layer deposition [42,43], spray pyrolysis [44,45], reactive or non-reactive magnetron sputtering [46–48], reactive electron beam evaporation [49], chemical vapor deposition [50,51], laser or plasma molecular-beam epitaxy [52–55], and electrodeposition [56] have been employed. Sol–gel, in particular, is a potential method with several advantages such as simple and low-cost processing, low processing temperatures, great purity and super-uniformity of the films, and controllability for the size and shape of sol particles [40,41]. Above all, sol-gel has two unique strong-points; one is a top-down process enabling the production of the size and shape of particles, and the other is the capability of coating the diverse applications with non-flat surfaces. These abilities are essential to achieve the acceptable performance of antibacterial films.

As well as the fabrication method of antibacterial films, the surrounding environment can affect their properties, and hence functional performance. In particular, a harsh application environment, —such as corrosive, wearable, frictional, and detachable conditions—can degrade the antimicrobial properties of the applied antibacterial film and even make them lose their functionality. Therefore, the functional durability of antibacterial films is required for their reliability and long lifetime (i.e., economic efficiency) in a practical environment.

Currently, it is being attempted to synergistically enhance the sterilization performance of ozone disinfection systems using antibacterial films in the systems. Ozone disinfectors are commercially used due to their safe, fast, and effective sterilization. An ozone sterilizer produces ozone gas through the following common process: oxygen gas is injected into the system chamber and then subjected to an electrical discharge, which decomposes oxygen molecules into monatomic oxygen and then reforms into ozone. The generated ozone—as a strong oxidizer—quickly kills even tough and resistant pathogenic bacteria. Simultaneously, the ozone providing oxidative stress can degrade or even lose functionality in the applied antibacterial films. Accordingly, it should first be determined whether the performance of the antibacterial film is sustainable in ozone conditions. Unfortunately, there are very few reports describing the ozone effect on antibacterial films [57,58].

In this paper, as a function of UVO exposure time, ZnO antibacterial film prepared by a simple spin-coating method was investigated with respect to the stability in the surface morphology, transmittance/absorbance, chemical state, and antibacterial activity by using field emission scanning electron microscopy (FE-SEM), ultraviolet–visible spectroscopy (UV-Vis), and X-ray photoelectron spectroscopy (XPS).

2. Materials and Methods

2.1. Preparation of the ZnO Film

ZnO films were prepared by a commonly-used sol-gel method reported in [59–62], as illustrated in Figure 1. ZnO solution was fabricated by dissolving 1.64 g zinc acetate dihydrate ($Zn(CH_3COO)_2{\cdot}2H_2O$) in the mixed solution of 10 g 2-methoxyethanol ($CH_3OC_2H_5OH$) and 0.5 g mono-ethanolamine ($HOCH_2CH_2NH_2$, MEA). The MEA was utilized as an organic stabilizer. The zinc acetate dihydrate was completely dissolved via 20-min ultrasonic vibration until no sediment was visible. Then, the transparent solution was filtered using a 0.45-μm membrane filter to obtain a ZnO precursor sol-type solution without any precipitates. To synthesize a uniform ZnO film, the precursor solution was spin-coated on a glass at 1500 revolutions per minute (rpm) for 30 s. The used glass had been

ultrasonically cleaned in a glass container of acetone and isopropyl alcohol for 10 min, respectively, and was successively dried at 150 °C for 1 min to volatilize the solvent and organic residuals.

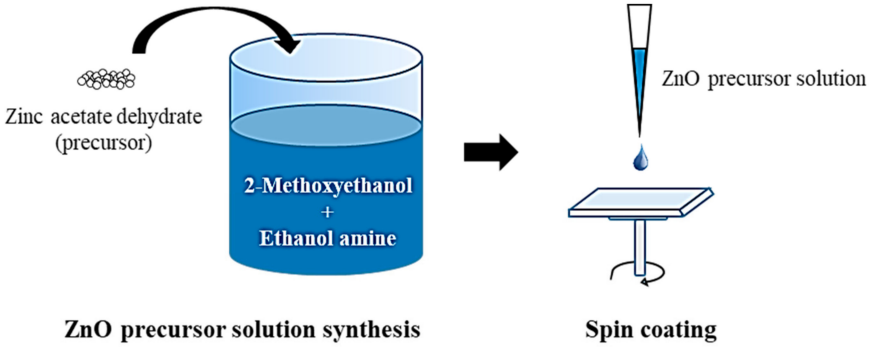

Figure 1. Schematic representation of the sol-gel fabrication process used to obtain the ZnO thin film.

2.2. UV–Ozone Treatment

For the prepared ZnO films, the UVO treatment of 0, 10, 30, 60, and 120 min was carried out using a commercial UVO cleaner (YOC130326, YUILUV co., Incheon, South Korea) containing UV light sources, a chamber, and injection and exhaust lines. The used UV light source was 185/254 nm from 150 W mercury lamps. The prepared ZnO samples were placed at a position of approximately 2 cm from the UV lamps. At that distance, the intensity of the generated UV light reaches 40 mW/cm^2. Hereafter, the synthesized ZnO film is referred to as "ZnO," and the UVO-treated ZnO films are denoted as "treatment time UVO ZnO" (e.g., 10-min UVO ZnO).

2.3. Characterization

The thickness and surface morphology of the ZnO samples were analyzed via a stylus profilometer (DektakXT, Bruker co., Billerica, Germany) and a SEM (JSM-7610F, JEOL co., Akishima, Japan), respectively. To investigate the chemical state, an XPS (K-Alpha, Thermo Fisher co., Waltham, USA) consisting of an X-ray source of 1.5 keV, an Al Kα monochromator, and a 128-channel detector was used. The transmission/absorption analysis was conducted using a UV-Vis (Cary 5000 UV-Vis-NIR, Agilent co., Santa Clara, CA, USA). The blank baseline of the UV-Vis had been set with air, and then the transmission and absorption spectrum were recorded in the wavelength range of 200 to 800 nm.

2.4. Antibacterial Test

According to the Japanese Industrial Standard (JIS) Z 2801 [63], the antibacterial activity of the prepared and UVO-treated ZnO films against *Staphylococcus aureus* ATCC 6538P (*S. aureus*) and *Escherichia coli* ATCC 8739 (*E. coli*) were evaluated. In brief, 0.1–0.4 ml of a bacterial culture of 10^5 to 10^6 colony-forming units per ml (CFU/ml) was injected onto a test plane of a 5 × 5 cm sample. The test plane was covered with a sterilized ethylene film of 4 × 4 cm and successively incubated in a petri dish at (35 ± 1) °C for 2, 4, or 24 h under a humid environment of 90% relative humidity (to prevent sterilization by desiccation). Immediately after the incubation, the test plane and cover film were sufficiently washed off with 10 ml SCDLP broth medium (i.e., an extraction solution). Exactly 1 ml of the washing liquid taken by a measuring pipette was injected in a test tube containing 9 mL phosphate-buffered saline and then sufficiently mixed by shaking the tube. The resulting dilution was spread in a sterile petri dish and subsequently intermixed with 15–20 ml plate count agar warmed up to 46–48 °C. After the complete solidification of the culture medium, the petri dish was turned upside down and incubated in an incubation chamber at (35 ± 1) °C for 40–48 h. Right after the incubation, the bacterial colonies in each petri dish were counted visually. To improve the reliability, this antibacterial test was performed in triplicate for each sample.

3. Results and Discussion

3.1. Morphological, Optical, and Chemical Properties

As identified by a stylus-profilometry measurement and SEM surface low-magnification image analysis, the synthesized ZnO film showed 36-nm thickness and surface continuity without micro-scaled agglomeration. After UVO treatment, its surface continuity was sustained, while the nanoscale surface morphology changed, as presented in the SEM high-magnification top-view image of Figure 2a. As can be seen in Figure 2a,b, the pores over the ZnO film surface decreased in size but increased in density and quantity as the UVO treatment proceeded. The surface porosity values, marked as points in the graph of Figure 2b, were obtained by calculating the pore area fraction of each Figure 2a image using the widely-used image analysis program, "ImagJ". With longer UVO treatment, the ZnO sol-gel film possessed a higher surface porosity and, hence, greater bactericidal activity. Some recent publications [10,14,15] have revealed experimentally that the functional performance of ZnO antibacterial coating against various bacterial strains is in proportion to the specific surface area, which is because of its surface-dependent antibacterial mechanisms mentioned in the introduction.

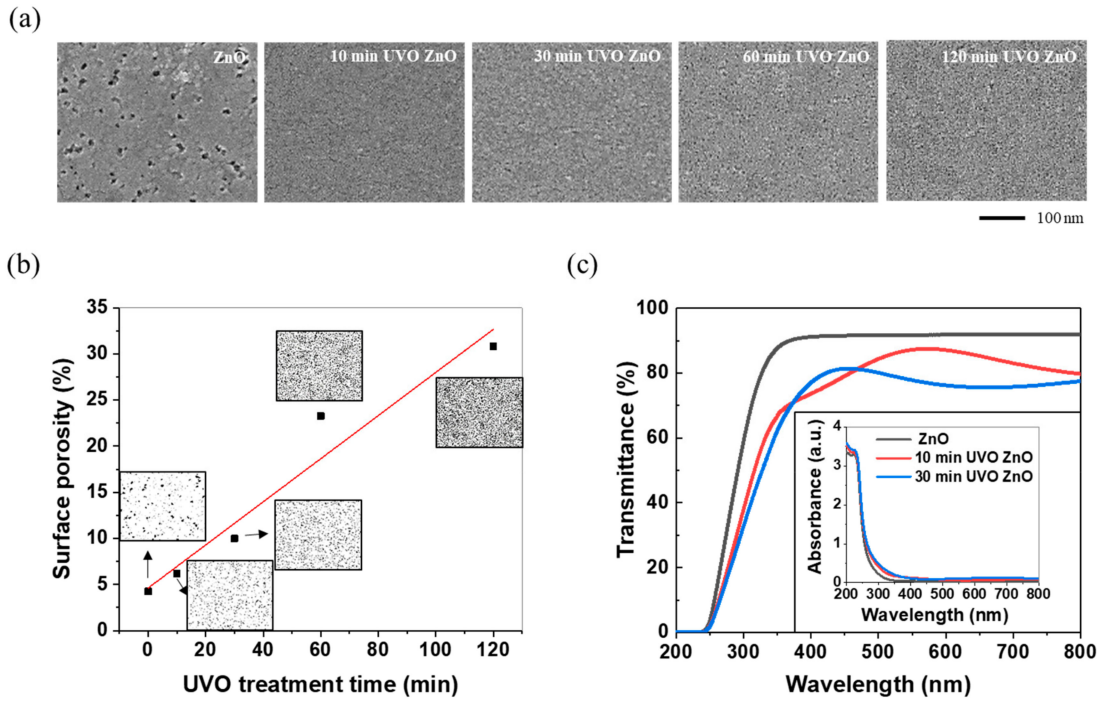

Figure 2. (**a**) SEM top-view images in secondary-electron image mode, (**b**) SEM image-based surface porosity, and (**c**) UV-Vis transmittance and absorbance spectrum of ZnO and UVO ZnO samples.

In addition to the antibacterial activity, optical properties can be affected by the surface structure. As displayed in Figure 2c, the synthesized ZnO film only absorbed UV light and had good transmittance of visible light and near infrared wavelengths; however, all the UVO ZnO samples displayed broad optical absorption, extending to the near infrared region of 800 nm. This optical change was consistent with the visual observation that the transparent synthesized ZnO film became slightly opaque after UVO exposure. In general, porous or rough surfaces tend to cause scattering of incident visible light, leading to a reduction in the transmittance and an increase in the probability of light absorption [64]. It has also demonstrated experimentally that a porous ZnO film prepared by the sol-gel/dipping method showed a low transmittance in the visible light wavelength region, in comparison with a compact ZnO film [65]. Based on the absorbance-transmittance equation (i.e., $A = 2 - \log_{10} \%T$, where A is absorbance and %T is the transmittance percentage), the ZnO porous film can be deduced to show a greater absorbance. In addition, the experimental observation, which showed that the absorbance of

the ZnO film in the UV wavelength slightly increased with the increasing UVO treatment time is in good agreement with the experimental results on nanostructured ZnO thin film by Ghamsari et al. [39].

As seen in Figure 3a Zn-O phase can be indirectly identified from the Zn and O peaks. ZnO (zinc monoxide) with a high thermodynamic stability is believed to be formed, which was experimentally demonstrated by X-ray diffraction analysis in a research [61] where ZnO film were fabricated in almost the same manner as in this study. Figure 3b,c shows the high-resolution spectrum of the ZnO and UVO ZnO samples in the energy range of the O 1s core-level, revealing the chemical composition and chemical state of the O element present within the sample surface (usually the top 10 nm based on the inherently limited analysis-depth of XPS). The energy scale for all the XPS spectrums was properly calibrated by fixing the C 1s level into 284.8 eV. As can be confirmed in Figure 3a, the O 1s peak can be divided into three peaks centered at 530.3, 531.6, and 532.2 eV. The main O 1s peak shifted to a lower binding-energy position from 532.2 to 531.6 eV, via a 10-min UVO treatment. After 30 min of UVO processing, a shoulder peak at 530.3 eV appeared for the first time. The smallest energy level peak at 530.3 eV (denoted as Zn-OH in Figure 3) is assigned to the oxygen atoms in zinc hydroxide ($Zn(OH)_2$) [66–68], and the other peaks at 531.6 (Zn-O) and 532.2 eV (V_O) are associated with the oxygen atoms in ZnO with and without oxygen vacancies, respectively [69–72]. Hence, it can be interpreted that the $Zn(OH)_2$ in the synthesized ZnO sample was fully transformed into ZnO with some oxygen vacancies during the first 10-min UVO treatment, and afterwards the oxygen vacancies were filled with oxygen atoms (i.e., oxygen uptake occurred). As identified from the peak-fitting results of Figure 3b, 24.2% of the oxygen vacancies were filled throughout 30-min UVO treatment. The experimental peak was deconvoluted by fitting the peak with a mixed Gaussian–Lorentz function.

In reality, ZnO films synthesized by using a $Zn(CH_3COO)_2{\cdot}2H_2O$ precursor (as in this study) can contain some $Zn(OH)_2$, which can be acceptable when considering the synthesis-associated chemical chain reactions [38,69,73–77]:

$$Zn(CH_3COO)_2{\cdot}2H_2O \rightarrow Zn(CH_3COO)_2 + 2H_2O \quad (1)$$

$$Zn(CH_3COO)_2 + 2H_2O \rightarrow 2CH_3COOH + Zn(OH)_2 \quad (2)$$

$$Zn(OH)_2 + 4NH_2CH_2CH_2OH \rightarrow [Zn(NH_2CH_2CH_2OH)_4]^{2+} + 2OH^- \quad (3)$$

$$Zn(OH)_2 + 2OH^- \rightarrow [Zn(OH)_4]^{2-} \quad (4)$$

$$Zn(OH)_2 \rightarrow ZnO + H_2O \quad (5)$$

$Zn(OH)_2$ can be generated as an intermediate in the course of the synthesis. From the thermogravimetric and differential thermal analysis (TG/DTA) result reported in [78], the thermal decomposition from $Zn(OH)_2$ to ZnO and water (Equation (5)) took place at a temperature range of 110–140 °C. However, in the case of the short (1 min) drying time at 150 °C in this study, it is suspected that the $Zn(OH)_2$ present in the spin-coated ZnO film was not totally decomposed to ZnO throughout the drying. Moreover, according to the documented TG/DTA results of ZnO sample [79,80], it was observed that the solvent (i.e., 2-methoxyethanol) and water remaining over the ZnO sample volatilized at 66 and 133 °C, respectively. On the other hand, structural decomposition of the hydroxyl group (i.e., $Zn(OH)_2$) occurred at a relatively higher temperature, 297 °C. Consequently, it is expected that some $Zn(OH)_2$ remained in the surface and/or inside of the synthesized ZnO film in this study. This is in agreement with other experimental results of ZnO sol-gel films fabricated by using a $Zn(CH_3COO)_2{\cdot}2H_2O$ precursor at a low processing temperature [59,81].

As depicted in Figure 3a, the $Zn(OH)_2$ was transformed into ZnO during UVO treatment, which is presumed to enhance the antibacterial activity. Fiedot et al. [82] reported that ZnO microrods deposited on PET mesh by a chemical bath deposition method contained a different amount of $Zn(OH)_2$ depending on the deposition temperature. The higher the ratio of ZnO to $Zn(OH)_2$, the greater the antimicrobial activity against *E. coli*, *S. aureus*, *Staphylococcus epidermidis*, and *Candida albicans*.

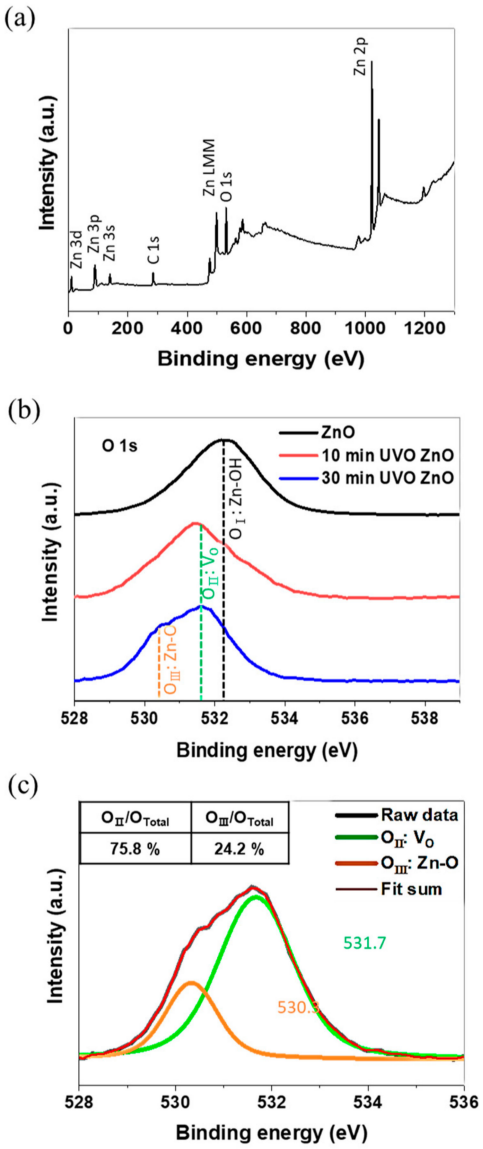

Figure 3. Baseline-corrected high-resolution XPS spectrum: (**a**) wide-scan spectrum of the 30-min UVO ZnO film, (**b**) comparison among ZnO and UVO ZnO films at the O 1s energy level, and (**c**) the high-resolution deconvoluted O 1s spectrum of the 30-min UVO ZnO film.

Additionally, the oxidation (more precisely, oxygen uptake) of the ZnO film in the UVO process can be explained. Once compressed air is supplied into the chamber of the used UVO cleaner, atomic oxygen is dissociated by 185 nm UV radiation, and, afterwards, ozone is continuously produced by 254 nm radiation [83–88], as follows:

$$O_2 + hv(185\ nm) \rightarrow O(3p) + O(3p), \quad (6)$$

$$O(3p) + O_2 + O_2 \rightarrow O_3 + O_2, \quad (7)$$

$$O_3 + hv(254\ nm) \rightarrow O(1d) + O_2. \quad (8)$$

As can be seen in Equations (6) and (8), ozone (O_3) and oxygen free radicals (O(3p) and O(1d)), which are a type of ROS (i.e., strong oxidants), were believed to be generated during UVO treatment. Thus, it is predicted that the resulting ROS caused the oxidation phenomena (i.e., oxygen uptake) of the ZnO film.

3.2. Bactericidal Effectiveness

In order to evaluate the antibacterial activity of the prepared ZnO sol-gel film as a function of the contact time and UVO treatment time, antibacterial tests were carried out according to the JIS Z 2801 standard [63]. The test organisms used in this study were *S. aureus* and *E. coli*, which are gram-positive and gram-negative bacterial strains, respectively. To achieve repeatability and reproducibility, each antibacterial test was validated in accordance with the guideline documented in the JIS Z 2801 standard [63].

Figure 4a,b and Table 1 show the test results of the synthesized ZnO film. The control sample (i.e., bare glass without ZnO film) showed that some of the test strain was killed up to the first 4-h incubation time; however, the test strain proliferated after 24 h. Compared to the control, the synthesized ZnO film exhibited superior antibacterial activity, killing 99.8% or 99.9% (4-log reduction for *S. aureus* and 6-log reduction for *E. coli*) of both test bacterial strains—irrespective of the incubation time. Given the antibacterial test results of other metal-oxide agents such as ZnO_2 [89], SiO_2 [90], and TiO_2 [91], the ZnO sol-gel film in this paper is estimated to be an excellent agent. Furthermore, satisfactory antibacterial activity of the synthesized ZnO sol-gel film was maintained even after the 120-min UVO treatment, as displayed in Figure 4c. Thus, it can be concluded that the performance sustainability of the ZnO film is excellent under ozone environments.

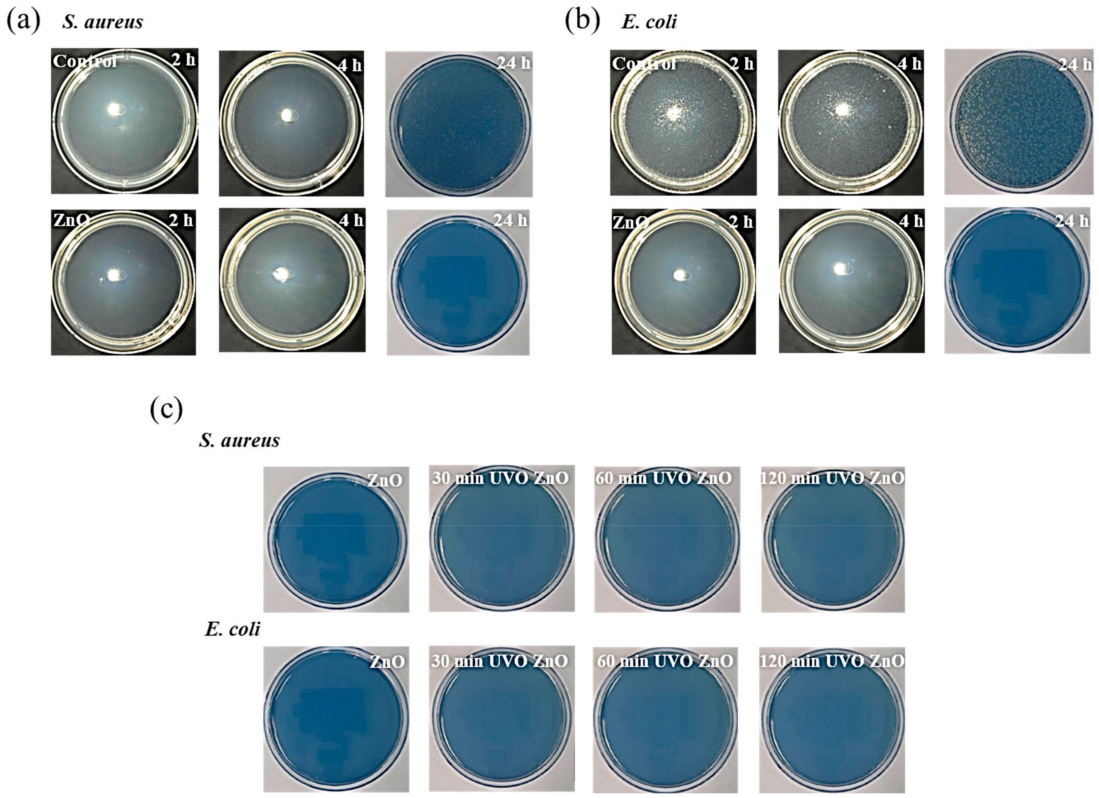

Figure 4. Antibacterial test (JIS Z 2801) results of the prepared ZnO film against *S. aureus* (gram-negative bacteria) and *E. coli* (gram-negative bacteria) for ZnO film, in terms of the (**a**,**b**) contact time and (**c**) UVO exposure time (the contact time was fixed as 24 h).

Table 1. Antibacterial activity of ZnO film as a function of the UVO treatment time, test bacteria, and contact time.

	Percent reduction (%)					
Test Organism	***S. aureus***			***E. coli***		
Contact Time	**2 h**	**4 h**	**24 h**	**2 h**	**4 h**	**24 h**
ZnO	99.9	99.9	99.9	99.8	99.9	99.9
30-min UVO ZnO	–	–	99.9	–	–	99.9
60-min UVO ZnO	–	–	99.9	–	–	99.9
120-min UVO ZnO	–	–	99.8	–	–	99.9
Control	2.0	0.6	−41.2	6.0	52.0	−7547.1

4. Conclusions

Our study experimentally demonstrated that a ZnO film prepared by a sol-gel/spin-coating method morphologically, optically, and chemically changed as a function of the UVO treatment time. However, the antibacterial ability of the film was sustained. The key findings and conclusions are as follows:

1. As the UVO treatment progressed, the film surface showed a decrease in the porosity size and an enormous increase in the porosity density, eventually resulting in an increase in the surface porosity and, thus, the specific surface area. The resulting surface, which was more porous, induced lower transmittance and higher absorbance in the visible light region.
2. O 1s XPS spectrum analysis revealed that the chemical state of the film surface also changed via UVO treatment. Firstly, the $Zn(OH)_2$ present in the prepared ZnO sol-gel film was transformed into ZnO containing oxygen vacancies. Afterwards, the oxygen vacancies were partially occupied with oxygen atoms as a consequence of ROS generation during UVO treatment. That is, a solid–solid transformation (or a dehydration reaction) and an oxidation reaction sequentially occurred on the ZnO film surface.
3. However, the UVO treatment-induced changes over the ZnO film surface did not degrade its antibacterial effectiveness against *S. aureus* and *E. coli*. Rather, the porosification and $Zn(OH)_2$ to ZnO transformation induced by the UVO treatment improved the bactericidal ability due to the specific surface area increase and the great antibacterial activity of ZnO being superior to that of $Zn(OH)_2$.

Given these experimental results, it can be deduced that the ZnO sol-gel antibacterial film is a potential way to synergistically improve commercially-used ozone disinfection systems for a long service time.

Author Contributions: Conceptualization, C.S.K., J.K., and S.L.; methodology, C.S.K. and J.K.; formal analysis, J.K.; investigation, J.K. and J.M.; data curation, J.K.; writing—original draft preparation, J.K.; writing—review and editing, J.K.; visualization, J.K.; supervision, C.S.K., S.L., and S.J.; project administration, C.S.K. and S.L.; funding acquisition, C.S.K. and S.L.

Funding: This research was supported by the fundamental research program (PNK6180) of the Korea Institute of Materials Science (KIMS).

Conflicts of Interest: The authors declare no conflict of interest.

References

1. McBryde, E.S.; Bradley, L.C.; Whitby, M.; McElwain, D.L.S. An investigation of contact transmission of methicillin-resistant Staphylococcus aureus. *J. Hosp. Infect.* **2004**, *58*, 104–108. [CrossRef] [PubMed]
2. Klevens, R.M.; Edwards, J.R.; Richards, C.L.; Horan, T.C.; Gaynes, R.P.; Pollock, D.A.; Cardo, D.M. Estimating health care-associated infections and deaths in U.S. Hospitals, 2002. *Public Health Rep.* **2007**, *122*, 160–166. [CrossRef] [PubMed]

3. Rutledge-Taylor, K.; Matlow, A.; Gravel, D.; Embree, J.; Le Saux, N.; Johnston, L.; Suh, K.; Embil, J.; Henderson, E.; John, M.; et al. A point prevalence survey of health care-associated infections in Canadian pediatric inpatients. *Am. J. Infect. Control* **2012**, *40*, 491–496. [CrossRef] [PubMed]
4. Peleg, A.Y.; Hooper, D.C. Hospital-acquired infections due to gram-negative bacteria. *N. Engl. J. Med.* **2010**, *362*, 1804–1813. [CrossRef] [PubMed]
5. Zarb, P.; Coignard, B.; Griskeviciene, J.; Muller, A.; Vankerckhoven, V.; Weist, K.; Goossens, M.M.; Vaerenberg, S.; Hopkins, S.; Catry, B.; et al. The european centre for disease prevention and control (ECDC) pilot point prevalence survey of healthcare-associated infections and antimicrobial use. *Eurosurveillance* **2012**, *17*, 20316. [CrossRef] [PubMed]
6. Allegranzi, B.; Nejad, S.B.; Combescure, C.; Graafmans, W.; Attar, H.; Donaldson, L.; Pittet, D. Burden of endemic health-care-associated infection in developing countries: Systematic review and meta-analysis. *Lancet* **2011**, *377*, 228–241. [CrossRef]
7. Siempos, I.I.; Fragoulis, K.N.; Falagas, M.E. World wide web resources on control of nosocomial infections. *Crit. Care* **2007**, *11*, 101–105. [CrossRef] [PubMed]
8. WHO's first global report on antibiotic resistance reveals serious, worldwide threat to public health. Available online: https://www.who.int/mediacentre/news/releases/2014/amr-report/en/ (accessed on 29 July 2019).
9. Yamamoto, O. Influence of particle size on the antibacterial activity of zinc oxide. *Int. J. Inorg. Mater.* **2001**, *3*, 643–646. [CrossRef]
10. Sirelkhatim, A.; Mahmud, S.; Seeni, A.; Kaus, N.H.M.; Ann, L.C.; Bakhori, S.K.M.; Hasan, H.; Mohamad, D. Review on zinc oxide nanoparticles: Antibacterial activity and toxicity mechanism. *Nano-Micro Lett.* **2015**, *7*, 219–242. [CrossRef] [PubMed]
11. Sawai, J.; Kawada, E.; Kanou, F.; Igarashi, H.; Hashimoto, A.; Kokugan, T.; Shimizu, M. Detection of active oxygen generated from ceramic powders having antibacterial activity. *J. Chem. Eng. Japan* **1996**, *29*, 627–633. [CrossRef]
12. Raghupathi, K.R.; Koodali, R.T.; Manna, A.C. Size-dependent bacterial growth inhibition and mechanism of antibacterial activity of zinc oxide nanoparticles. *Langmuir* **2011**, *27*, 4020–4028. [CrossRef] [PubMed]
13. Azam, A.; Ahmed, A.S.; Oves, M.; Khan, M.S.; Habib, S.S.; Memic, A. Antimicrobial activity of metal oxide nanoparticles against Gram-positive and Gram-negative bacteria: A comparative study. *Int. J. Nanomedicine* **2012**, *122*, 160–166. [CrossRef] [PubMed]
14. Stanković, A.; Dimitrijević, S.; Uskoković, D. Influence of size scale and morphology on antibacterial properties of ZnO powders hydrothemally synthesized using different surface stabilizing agents. *Colloids Surfaces B Biointerfaces* **2013**, *102*, 21–28. [CrossRef] [PubMed]
15. Appierot, G.; Lipovsky, A.; Dror, R.; Perkas, N.; Nitzan, Y.; Lubart, R.; Gedanken, A. Enhanced antibacterial actiwity of nanocrystalline ZnO due to increased ROS-mediated cell injury. *Adv. Funct. Mater.* **2009**, *19*, 842–852. [CrossRef]
16. Chang, Y.N.; Zhang, M.; Xia, L.; Zhang, J.; Xing, G. The toxic effects and mechanisms of CuO and ZnO nanoparticles. *Materials (Basel)* **2012**, *5*, 2850–2871. [CrossRef]
17. Nair, S.; Sasidharan, A.; Divya Rani, V.V.; Menon, D.; Nair, S.; Manzoor, K.; Raina, S. Role of size scale of ZnO nanoparticles and microparticles on toxicity toward bacteria and osteoblast cancer cells. *J. Mater. Sci. Mater. Med.* **2008**, *20*, 235–241. [CrossRef]
18. Azam, A.; Ahmed, A.S.; Oves, M.; Khan, M.S.; Memic, A. Size-dependent antimicrobial properties of CuO nanoparticles against Gram-positive and -negative bacterial strains. *Int. J. Nanomedicine* **2012**, *7*, 3527. [CrossRef]
19. Gupta, K.; Singh, R.P.; Pandey, A.; Pandey, A. Photocatalytic antibacterial performance of TiO_2 and Ag-doped TiO_2 against S. Aureus. P. Aeruginosa and E. Coli. *Beilstein J. Nanotechnol.* **2013**, *4*, 345–351. [CrossRef]
20. Allahverdiyev, A.M.; Abamor, E.S.; Bagirova, M.; Rafailovich, M. Antimicrobial effects of TiO(2) and Ag(2)O nanoparticles against drug-resistant bacteria and leishmania parasites. *Future Microbiol.* **2011**, *6*, 933–940. [CrossRef]
21. He, Y.; Ingudam, S.; Reed, S.; Gehring, A.; Strobaugh, T.P.; Irwin, P. Study on the mechanism of antibacterial action of magnesium oxide nanoparticles against foodborne pathogens. *J. Nanobiotechnology* **2016**, *14*, 54. [CrossRef]
22. Jin, T.; He, Y. Antibacterial activities of magnesium oxide (MgO) nanoparticles against foodborne pathogens. *J. Nanoparticle Res.* **2011**, *13*, 6877–6885. [CrossRef]

23. Pal, S.; Tak, Y.K.; Song, J.M. Does the antibacterial activity of silver nanoparticles depend on the shape of the nanoparticle? A study of the gram-negative bacterium Escherichia coli. *J. Biol. Chem.* **2015**, *73*, 1712–1720. [CrossRef] [PubMed]
24. Brayner, R.; Ferrari-Iliou, R.; Brivois, N.; Djediat, S.; Benedetti, M.F.; Fiévet, F. Toxicological impact studies based on Escherichia coli bacteria in ultrafine ZnO nanoparticles colloidal medium. *Nano Lett.* **2006**, *6*, 866–870. [CrossRef] [PubMed]
25. Jones, N.; Ray, B.; Ranjit, K.T.; Manna, A.C. Antibacterial activity of ZnO nanoparticle suspensions on a broad spectrum of microorganisms. *FEMS Microbiol. Lett.* **2008**, *279*, 71–76. [CrossRef] [PubMed]
26. Jalal, R.; Goharshadi, E.K.; Abareshi, M.; Moosavi, M.; Yousefi, A.; Nancarrow, P. ZnO nanofluids: Green synthesis, characterization, and antibacterial activity. *Mater. Chem. Phys.* **2010**, *121*, 198–201. [CrossRef]
27. Seil, J.T.; Webster, T.J. Antimicrobial applications of nanotechnology: Methods and literature. *Int. J. Nanomedicine* **2012**, *7*, 2767. [PubMed]
28. Zarrindokht Emami-Karvani Antibacterial activity of ZnO nanoparticle on Gram-positive and Gram-negative bacteria. *African J. Microbiol. Res.* **2012**, *5*, 1368–1373.
29. Padmavathy, N.; Vijayaraghavan, R. Enhanced bioactivity of ZnO nanoparticles-an antimicrobial study. *Sci. Technol. Adv. Mater.* **2008**, *9*, 035004. [CrossRef]
30. Colon, G.; Ward, B.C.; Webster, T.J. Increased osteoblast and decreased Staphylococcus epidermidis functions on nanophase ZnO and TiO_2. *J. Biomed. Mater. Res. Part A* **2006**, *78*, 595–604. [CrossRef]
31. Kasemets, K.; Ivask, A.; Dubourguier, H.C.; Kahru, A. Toxicity of nanoparticles of ZnO, CuO and TiO_2 to yeast Saccharomyces cerevisiae. *Toxicol. Vitr.* **2009**, *23*, 1116–1122. [CrossRef]
32. Brunner, T.J.; Wick, P.; Manser, P.; Spohn, P.; Grass, R.N.; Limbach, L.K.; Bruinink, A.; Stark, W.J. In vitro cytotoxicity of oxide nanoparticles: Comparison to asbestos, silica, and the effect of particle solubility. *Environ. Sci. Technol.* **2006**, *40*, 4374–4381. [CrossRef] [PubMed]
33. Li, M.; Zhu, L.; Lin, D. Toxicity of ZnO nanoparticles to escherichia Coli: Mechanism and the influence of medium components. *Environ. Sci. Technol.* **2011**, *45*, 1977–1983. [CrossRef] [PubMed]
34. Adams, L.K.; Lyon, D.Y.; Alvarez, P.J.J. Comparative eco-toxicity of nanoscale TiO_2, SiO_2, and ZnO water suspensions. *Water Res.* **2006**, *40*, 3527–3532. [CrossRef] [PubMed]
35. Zhang, L.; Jiang, Y.; Ding, Y.; Povey, M.; York, D. Investigation into the antibacterial behaviour of suspensions of ZnO nanoparticles (ZnO nanofluids). *J. Nanoparticle Res.* **2007**, *9*, 479–489. [CrossRef]
36. Lipovsky, A.; Nitzan, Y.; Gedanken, A.; Lubart, R. Antifungal activity of ZnO nanoparticles-the role of ROS mediated cell injury. *Nanotechnology* **2011**, *22*, 105101. [CrossRef]
37. Zhang, L.; Ding, Y.; Povey, M.; York, D. ZnO nanofluids-A potential antibacterial agent. *Prog. Nat. Sci.* **2008**, *18*, 939–944. [CrossRef]
38. Sagar, P.; Shishodia, P.K.; Mehra, R.M. Influence of pH value on the quality of sol–gel derived ZnO films. *Appl. Surf. Sci.* **2007**, *253*, 5419–5424. [CrossRef]
39. Ghamsari, M.S.; Alamdari, S.; Han, W.; Park, H.H. Impact of nanostructured thin ZnO film in ultraviolet protection. *Int. J. Nanomedicine* **2017**, *12*, 207–216. [CrossRef]
40. Znaidi, L. Sol-gel-deposited ZnO thin films: A review. *Mater. Sci. Eng. B* **2010**, *174*, 18–30. [CrossRef]
41. Kamalasanan, M.N.; Chandra, S. Sol-gel synthesis of ZnO thin films. *Thin Solid Films* **1996**, *288*, 112–115. [CrossRef]
42. Tynell, T.; Karppinen, M. Atomic layer deposition of ZnO: A review. *Semicond. Sci. Technol.* **2014**, *29*, 043001. [CrossRef]
43. Yamada, A.; Sang, B.; Konagai, M. Atomic layer deposition of ZnO transparent conducting oxides. *Appl. Surf. Sci.* **1997**, *112*, 216–222. [CrossRef]
44. Abrarov, S.M.; Yuldashev, S.U.; Kim, T.W.; Lee, S.B.; Kwon, Y.H.; Kang, T.W. Effect of photonic band-gap on photoluminescence of ZnO deposited inside the green synthetic opal. *Opt. Commun.* **2005**, *250*, 111–119. [CrossRef]
45. Ayouchi, R.; Leinen, D.; Martin, F.; Gabas, M.; Dalchiele, E.; Ramos-Barrado, J.R. Preparation and characterization of transparent ZnO thin films obtained by spray pyrolysis. *Thin Solid Films* **2003**, *426*, 68–77. [CrossRef]
46. Martin, P.M.; Good, M.S.; Johnston, J.W.; Posakony, G.J.; Bond, L.J.; Crawford, S.L. Piezoelectric films for 100-MHz ultrasonic transducers. *Thin Solid Films* **2000**, *379*, 253–258. [CrossRef]

47. Hofman, G.L.; Domagala, R.F.; Copeland, G.L. Irradiation behavior of low-enriched U 6 Fe-Al dispersion fuel elements. *J. Nucl. Mater.* **1987**, *150*, 238–243. [CrossRef]
48. Ondo-Ndong, R.; Pascal-Delannoy, F.; Boyer, A.; Giani, A.; Foucaran, A. Structural properties of zinc oxide thin films prepared by r.f. magnetron sputtering. *Mater. Sci. Eng. B* **2003**, *97*, 68–73. [CrossRef]
49. Agarwal, D.C.; Chauhan, R.S.; Kumar, A.; Kabiraj, D.; Singh, F.; Khan, S.A.; Avasthi, D.K.; Pivin, J.C.; Kumar, M.; Ghatak, J.; et al. Synthesis and characterization of ZnO thin film grown by electron beam evaporation. *J. Appl. Phys.* **2006**, *99*, 123105. [CrossRef]
50. Chen, Z.; Shum, K.; Salagaj, T.; Zhang, W.; Strobl, K. ZnO thin films synthesized by chemical vapor deposition. In Proceedings of the 2010 IEEE Long Island Systems, Applications and Technology Conference, Farmingdale, NY, USA, 7 May 2010; IEEE: Piscataway, NJ, USA, 2010; pp. 1–6.
51. Tan, S.T.; Chen, B.J.; Sun, X.W.; Fan, W.J.; Kwok, H.S.; Zhang, X.H.; Chua, S.J. Blueshift of optical band gap in ZnO thin films grown by metal-organic chemical-vapor deposition. *J. Appl. Phys.* **2005**, *98*, 013505. [CrossRef]
52. Bagnall, D.M.; Chen, Y.F.; Shen, M.Y.; Zhu, Z.; Goto, T.; Yao, T. Room temperature excitonic stimulated emission from zinc oxide epilayers grown by plasma-assisted MBE. *J. Cryst. Growth* **1998**, *184*, 605–609. [CrossRef]
53. Yu, P.; Tang, Z.K.; Wong, G.K.L.; Kawasaki, M.; Ohtomo, A.; Koinuma, H.; Segawa, Y. Room-temperature gain spectra and lasing in microcrystalline ZnO thin films. *J. Cryst. Growth* **1998**, *184*, 601–604. [CrossRef]
54. Ohtomo, A.; Kawasaki, M.; Sakurai, Y.; Yoshida, Y.; Koinuma, H.; Yu, P.; Tang, Z.K.; Wong, G.K.L.; Segawa, Y. Room temperature ultraviolet laser emission from ZnO nanocrystal thin films grown by laser MBE. *Mater. Sci. Eng. B* **1998**, *54*, 24–28. [CrossRef]
55. Kawasaki, M.; Ohtomo, A.; Ohkubo, I.; Koinuma, H.; Tang, Z.K.; Yu, P.; Wong, G.K.L.; Zhang, B.P.; Segawa, Y. Excitonic ultraviolet laser emission at room temperature from naturally made cavity in ZnO nanocrytal thin films. *Mater. Sci. Eng. B* **1998**, *56*, 239–245. [CrossRef]
56. Pauporté, T.; Lincot, D. Electrodeposition of semiconductors for optoelectronic devices: Results on zinc oxide. *Electrochim. Acta* **2000**, *45*, 3345–3353. [CrossRef]
57. Dodd, M.C.; Kohler, H.P.E.; Gunten, U. Von Oxidation of antibacterial compounds by ozone and hydroxyl radical: Elimination of biological activity during aqueous ozonation processes. *Environ. Sci. Technol.* **2009**, *43*, 2498–2504. [CrossRef]
58. Guirguis, O.W.; El-Bassyouni, G.T.; Esawy, M.A.; Abd Elkader, N.R.; Mahmoud, H.M.; Mostafa, H.M.; Abdel-Zaher, N.A. Exposure of chitosan to UV/ozone, Structural information and antibacterial activity. *J. Appl. Pharm. Sci.* **2016**, *6*, 124–130. [CrossRef]
59. Li, J.; Yang, D.; Zhu, X. Effects of aging time and annealing temperature on structural and optical properties of sol-gel ZnO thin films. *Aip Adv.* **2017**, *7*, 65213. [CrossRef]
60. Khan, Z.R.; Khan, M.S.; Zulfequar, M.; Khan, M.S. Optical and structural properties of ZnO thin films fabricated by sol-gel method. *Mater. Sci. Appl.* **2011**, *2*, 340. [CrossRef]
61. Singh, A.; Kumar, A.; Suri, N.; Kumar, S.; Kumar, M.; Khanna, P.K.; Kumar, D. Structural and optical characterization of ZnO thin films deposited by sol-gel method. *J. Optoelectron. Adv. M.* **2009**, *11*, 790–793.
62. Gómez Núñez, A.; Alonso-Gil, S.; López, C.; Roura, P.; Vilà, A. Role of Ethanolamine on the Stability of a Sol-Gel ZnO Ink. *J. Phys. Chem.* **2017**, *121*, 23839–23846. [CrossRef]
63. JIS, Z. 2801: 2010 (SIAA/JSA) Antibacterial products—Test for antibacterial activity and efficacy. Available online: http://www.questin.org/sites/default/files/intl-codes/jis.z.2801.e.2010.pdf (accessed on 29 July 2019).
64. Go, H.; Han, E.-M.; Hee Kang, M.; Hyun Kim, Y.; Yun, C. The coated porous polyimide layers for optical scattering films. *AIMS Mater. Sci.* **2018**, *5*, 1102–1111. [CrossRef]
65. Liu, Z.; Jin, Z.; Li, W.; Liu, X. Ordered porous ZnO thin films formed by dip-coating method using PS templates. *J. Sol-Gel Sci. Technol.* **2006**, *40*, 25–30. [CrossRef]
66. Shin, H.; Kang, C.; Baek, K.-H.; Kim, J.Y.; Do, L.-M.; Lee, C. Low-temperature solution-processed zinc oxide field effect transistor by blending zinc hydroxide and zinc oxide nanoparticle in aqueous solutions. *Jpn. J. Appl. Phys.* **2018**, *57*, 05GD04. [CrossRef]
67. Karakawa, M.; Sugahara, T.; Hirose, Y.; Suganuma, K.; Aso, Y. Thin Film of Amorphous Zinc Hydroxide Semiconductor for Optical Devices with an Energy-Efficient Beneficial Coating by Metal Organic Decomposition Process. *Sci. Rep.* **2018**, *8*, 10839. [CrossRef]

68. Hsu, J.-C.; Lin, Y.-H.; Wang, P.W.; Chen, Y.Y. Spectroscopic ellipsometry studies on various zinc oxide films deposited by ion beam sputtering at room temperature. *Appl. Opt.* **2012**, *51*, 1209–1215. [CrossRef]
69. Sun, Y.; Seo, J.H.; Takacs, C.J.; Seifter, J.; Heeger, A.J. Inverted polymer solar cells integrated with a low-temperature-annealed sol-gel-derived ZnO film as an electron transport layer. *Adv. Mater.* **2011**, *23*, 1679–1683. [CrossRef]
70. Ghobadi, A.; Ulusoy, T.G.; Garifullin, R.; Guler, M.O.; Okyay, A.K. A heterojunction design of single layer hole tunneling ZnO passivation wrapping around TiO_2 nanowires for superior photocatalytic performance. *Sci. Rep.* **2016**, *6*, 30587. [CrossRef]
71. Jung, Y.; Yang, W.; Koo, C.Y.; Song, K.; Moon, J. High performance and high stability low temperature aqueous solution-derived Li–Zr co-doped ZnO thin film transistors. *J. Mater. Chem.* **2012**, *22*, 5390–5397. [CrossRef]
72. Kushwaha, A.; Aslam, M. Hydrogen-incorporated ZnO nanowire films: Stable and high electrical conductivity. *J. Phys. D. Appl. Phys.* **2013**, *46*, 485104. [CrossRef]
73. Znaidi, L.; Illia, G.S.; Benyahia, S.; Sanchez, C.; Kanaev, A. V Oriented ZnO thin films synthesis by sol–gel process for laser application. *Thin Solid Films* **2003**, *428*, 257–262. [CrossRef]
74. Jagadamma, L.K.; Abdelsamie, M.; El Labban, A.; Aresu, E.; Ndjawa, G.O.N.; Anjum, D.H.; Cha, D.; Beaujuge, P.M.; Amassian, A. Efficient inverted bulk-heterojunction solar cells from low-temperature processing of amorphous ZnO buffer layers. *J. Mater. Chem. A* **2014**, *2*, 13321–13331. [CrossRef]
75. Nehmann, J.B.; Ehrmann, N.; Reineke-Koch, R.; Bahnemann, D.W. Aluminum-doped zinc oxide sol–gel thin films: Influence of the sol's water content on the resistivity. *Thin Solid Films* **2014**, *556*, 168–173. [CrossRef]
76. Yang, F.; Kang, D.-W.; Kim, Y.-S. Improved interface of ZnO/$CH_3NH_3PbI_3$ by a dynamic spin-coating process for efficient perovskite solar cells. *RSC Adv.* **2017**, *7*, 19030–19038. [CrossRef]
77. Briois, V.; Giorgetti, C.; Baudelet, F.; Blanchandin, S.; Tokumoto, M.S.; Pulcinelli, S.H.; Santilli, C.V. Dynamical study of ZnO nanocrystal and Zn-HDS layered basic zinc acetate formation from sol− gel route. *J. Phys. Chem. C* **2007**, *111*, 3253–3258. [CrossRef]
78. Nistor, S.V.; Ghica, D.; Stefan, M.; Vlaicu, I.; Barascu, J.N.; Bartha, C. Magnetic defects in crystalline $Zn(OH)_2$ and nanocrystalline ZnO resulting from its thermal decomposition. *J. Alloys Compd.* **2013**, *548*, 222–227. [CrossRef]
79. Mihaiu, S.; Szilágyi, I.M.; Atkinson, I.; Mocioiu, O.C.; Hunyadi, D.; Pandele-Cusu, J.; Toader, A.; Munteanu, C.; Boyadjiev, S.; Madarász, J. Thermal study on the synthesis of the doped ZnO to be used in TCO films. *J. Therm. Anal. Calorim.* **2016**, *124*, 71–80. [CrossRef]
80. Stefan, M.; Ghica, D.; Nistor, S.V.; Maraloiu, A.V.; Plugaru, R. Mn^{2+} ions distribution in doped sol–gel deposited ZnO films. *Appl. Surf. Sci.* **2017**, *396*, 1880–1889. [CrossRef]
81. Rochman, N.T.; Akwalia, P.R. Fabrication and characterization of Zinc Oxide (ZnO) nanoparticle by sol-gel method. In Proceedings of the Journal of Physics: Conference Series, Surabaya, Indonesia, 27 October 2016; IOP Publishing: Bristol, UK, 2017; 853, p. 12041.
82. Fiedot, M.; Maliszewska, I.; Rac-Rumijowska, O.; Suchorska-Wózniak, P.; Lewínska, A.; Teterycz, H. The relationship between the mechanism of zinc oxide crystallization and its antimicrobial properties for the surface modification of surgical meshes. *Materials (Basel).* **2017**, *10*, 353. [CrossRef]
83. Urwyler, P.; Pascual, A.; Müller, B.; Schift, H. Ultraviolet–ozone surface cleaning of injection-molded, thermoplastic microcantilevers. *J. Appl. Polym. Sci.* **2015**, *132*. [CrossRef]
84. Vig, J.R. UV/ozone cleaning of surfaces. *J. Vac. Sci. Technol. Vacuum Surfaces Film* **1985**, *3*, 1027–1034. [CrossRef]
85. Wei, W.; Yang, C.; Mai, J.; Gong, Y.; Yan, L.; Zhao, K.; Ning, H.; Wu, S.; Gao, J.; Gao, X. High mobility solution-processed C 8-BTBT organic thin-film transistors via UV-ozone interface modification. *J. Mater. Chem. C* **2017**, *5*, 10652–10659. [CrossRef]
86. Summerfelt, S.T. Ozonation and UV irradiation—An introduction and examples of current applications. *Aquac. Eng.* **2003**, *28*, 21–36. [CrossRef]
87. Zoschke, K.; Börnick, H.; Worch, E. Vacuum-UV radiation at 185 nm in water treatment—A review. *Water Res.* **2014**, *52*, 131–145. [CrossRef]
88. Yasuda, K.; Okazaki, Y.; Abe, Y.; Tsuga, K. Effective UV/Ozone irradiation method for decontamination of hydroxyapatite surfaces. *Heliyon* **2017**, *3*, e00372. [CrossRef]

89. Catauro, M.; Barrino, F.; Bononi, M.; Colombini, E.; Giovanardi, R.; Veronesi, P.; Tranquillo, E. Coating of Titanium Substrates with ZrO_2 and ZrO_2-SiO_2 Composites by Sol-Gel Synthesis for Biomedical Applications: Structural Characterization, Mechanical and Corrosive Behavior. *Coatings* **2019**, *9*, 200. [CrossRef]
90. Tranquillo, E.; Barrino, F.; Dal Poggetto, G.; Blanco, I. Sol–Gel Synthesis of Silica-Based Materials with Different Percentages of PEG or PCL and High Chlorogenic Acid Content. *Materials (Basel)* **2019**, *12*, 155. [CrossRef]
91. Verdier, T.; Coutand, M.; Bertron, A.; Roques, C. Antibacterial activity of TiO_2 photocatalyst alone or in coatings on E. coli: The influence of methodological aspects. *Coatings* **2014**, *4*, 670–686. [CrossRef]